Independent measurement of the neutrino mixing angle θ_{13} via neutron capture on hydrogen at Daya Bay

F. P. An *et al.* (Daya Bay Collaboration)

Phys. Rev. D **90**, 071101 — Published 3 October 2014

DOI: 10.1103/PhysRevD.90.071101

Independent Measurement of the Neutrino Mixing Angle θ_{13} via Neutron Capture on Hydrogen at Daya Bay

F. P. An,[1] A. B. Balantekin,[2] H. R. Band,[2] W. Beriguete,[3] M. Bishai,[3] S. Blyth,[4] I. Butorov,[5] G. F. Cao,[6] J. Cao,[6] Y.L. Chan,[7] J. F. Chang,[6] L. C. Chang,[8] Y. Chang,[9] C. Chasman,[3] H. Chen,[6] Q. Y. Chen,[10] S. M. Chen,[11] X. Chen,[7] X. Chen,[6] Y. X. Chen,[12] Y. Chen,[13] Y. P. Cheng,[6] J. J. Cherwinka,[2] M. C. Chu,[7] J. P. Cummings,[14] J. de Arcos,[15] Z. Y. Deng,[6] Y. Y. Ding,[6] M. V. Diwan,[3] E. Draeger,[15] X. F. Du,[6] D. A. Dwyer,[16] W. R. Edwards,[16] S. R. Ely,[17] J. Y. Fu,[6] L. Q. Ge,[18] R. Gill,[3] M. Gonchar,[5] G. H. Gong,[11] H. Gong,[11] W. Q. Gu,[19] M. Y. Guan,[6] X. H. Guo,[20] R. W. Hackenburg,[3] G. H. Han,[21] S. Hans,[3] M. He,[6] K. M. Heeger,[2,22] Y. K. Heng,[6] P. Hinrichs,[2] Y. K. Hor,[23] Y. B. Hsiung,[4] B. Z. Hu,[8] L. M. Hu,[3] L. J. Hu,[20] T. Hu,[6] W. Hu,[6] E. C. Huang,[17] H. Huang,[24] X. T. Huang,[10] P. Huber,[23] G. Hussain,[11] Z. Isvan,[3] D. E. Jaffe,[3] P. Jaffke,[23] K. L. Jen,[8] S. Jetter,[6] X. P. Ji,[25] X. L. Ji,[6] H. J. Jiang,[18] J. B. Jiao,[10] R. A. Johnson,[26] L. Kang,[27] S. H. Kettell,[3] M. Kramer,[16,28] K. K. Kwan,[7] M.W. Kwok,[7] T. Kwok,[29] W. C. Lai,[18] K. Lau,[30] L. Lebanowski,[11] J. Lee,[16] R. T. Lei,[27] R. Leitner,[31] A. Leung,[29] J. K. C. Leung,[29] C. A. Lewis,[2] D. J. Li,[32] F. Li,[18,6] G. S. Li,[19] Q. J. Li,[6] W. D. Li,[6] X. N. Li,[6] X. Q. Li,[25] Y. F. Li,[6] Z. B. Li,[33] H. Liang,[32] C. J. Lin,[16] G. L. Lin,[8] P.Y. Lin,[8] S. K. Lin,[30] Y. C. Lin,[18] J. J. Ling,[3,17] J. M. Link,[23] L. Littenberg,[3] B. R. Littlejohn,[26] D. W. Liu,[30] H. Liu,[30] J. L. Liu,[19] J. C. Liu,[6] S. S. Liu,[29] Y. B. Liu,[6] C. Lu,[34] H. Q. Lu,[6] K. B. Luk,[28,16] Q. M. Ma,[6] X. Y. Ma,[6] X. B. Ma,[12] Y. Q. Ma,[6] K. T. McDonald,[34] M. C. McFarlane,[2] R.D. McKeown,[35,21] Y. Meng,[23] I. Mitchell,[30] J. Monari Kebwaro,[36] Y. Nakajima,[16] J. Napolitano,[37] D. Naumov,[5] E. Naumova,[5] I. Nemchenok,[5] H. Y. Ngai,[29] Z. Ning,[6] J. P. Ochoa-Ricoux,[38,16] A. Olshevski,[5] S. Patton,[16] V. Pec,[31] J. C. Peng,[17] L. E. Piilonen,[23] L. Pinsky,[30] C. S. J. Pun,[29] F. Z. Qi,[6] M. Qi,[39] X. Qian,[3] N. Raper,[40] B. Ren,[27] J. Ren,[24] R. Rosero,[3] B. Roskovec,[31] X. C. Ruan,[24] B. B. Shao,[11] H. Steiner,[28,16] G. X. Sun,[6] J. L. Sun,[41] Y. H. Tam,[7] X. Tang,[6] H. Themann,[3] K. V. Tsang,[16] R. H. M. Tsang,[35] C.E. Tull,[16] Y. C. Tung,[4] B. Viren,[3] V. Vorobel,[31] C. H. Wang,[9] L. S. Wang,[6] L. Y. Wang,[6] M. Wang,[10] N. Y. Wang,[20] R. G. Wang,[6] W. Wang,[21,33] W. W. Wang,[39] X. Wang,[42] Y. F. Wang,[6] Z. Wang,[11] Z. Wang,[6] Z. M. Wang,[6] D. M. Webber,[2] H. Y. Wei,[11] Y. D. Wei,[27] L. J. Wen,[6] K. Whisnant,[43] C. G. White,[15] L. Whitehead,[30] T. Wise,[2] H. L. H. Wong,[28,16] S. C. F. Wong,[7] E. Worcester,[3] Q. Wu,[10] D. M. Xia,[6] J. K. Xia,[6] X. Xia,[10] Z. Z. Xing,[6] J. Y. Xu,[7] J. L. Xu,[6] J. Xu,[20] Y. Xu,[25] T. Xue,[11] J. Yan,[36] C. C. Yang,[6] L. Yang,[27] M. S. Yang,[6] M. T. Yang,[10] M. Ye,[6] M. Yeh,[3] Y. S. Yeh,[8] B. L. Young,[43] G. Y. Yu,[39] J. Y. Yu,[11] Z. Y. Yu,[6] S. L. Zang,[39] B. Zeng,[18] L. Zhan,[6] C. Zhang,[3] F. H. Zhang,[6] J. W. Zhang,[6] Q. M. Zhang,[36] Q. Zhang,[18] S. H. Zhang,[6] Y. C. Zhang,[32] Y. M. Zhang,[11] Y. H. Zhang,[6] Y. X. Zhang,[41] Z. J. Zhang,[27] Z. Y. Zhang,[6] Z. P. Zhang,[32] J. Zhao,[6] Q. W. Zhao,[6] Y. Zhao,[12,21] Y. B. Zhao,[6] L. Zheng,[32] W. L. Zhong,[6] L. Zhou,[6] Z. Y. Zhou,[24] H. L. Zhuang,[6] and J. H. Zou[6]

(Daya Bay Collaboration)

[1] *Institute of Modern Physics, East China University of Science and Technology, Shanghai*
[2] *University of Wisconsin, Madison, Wisconsin, USA*
[3] *Brookhaven National Laboratory, Upton, New York, USA*
[4] *Department of Physics, National Taiwan University, Taipei*
[5] *Joint Institute for Nuclear Research, Dubna, Moscow Region*
[6] *Institute of High Energy Physics, Beijing*
[7] *Chinese University of Hong Kong, Hong Kong*
[8] *Institute of Physics, National Chiao-Tung University, Hsinchu*
[9] *National United University, Miao-Li*
[10] *Shandong University, Jinan*
[11] *Department of Engineering Physics, Tsinghua University, Beijing*
[12] *North China Electric Power University, Beijing*
[13] *Shenzhen University, Shenzhen*
[14] *Siena College, Loudonville, New York, USA*
[15] *Department of Physics, Illinois Institute of Technology, Chicago, Illinois, USA*
[16] *Lawrence Berkeley National Laboratory, Berkeley, California, USA*
[17] *Department of Physics, University of Illinois at Urbana-Champaign, Urbana, Illinois, USA*
[18] *Chengdu University of Technology, Chengdu*
[19] *Shanghai Jiao Tong University, Shanghai*
[20] *Beijing Normal University, Beijing*
[21] *College of William and Mary, Williamsburg, Virginia, USA*
[22] *Department of Physics, Yale University, New Haven, Connecticut, USA*
[23] *Center for Neutrino Physics, Virginia Tech, Blacksburg, Virginia, USA*
[24] *China Institute of Atomic Energy, Beijing*
[25] *School of Physics, Nankai University, Tianjin*

[26]Department of Physics, University of Cincinnati, Cincinnati, Ohio, USA
[27]Dongguan University of Technology, Dongguan
[28]Department of Physics, University of California, Berkeley, California, USA
[29]Department of Physics, The University of Hong Kong, Pokfulam, Hong Kong
[30]Department of Physics, University of Houston, Houston, Texas, USA
[31]Charles University, Faculty of Mathematics and Physics, Prague
[32]University of Science and Technology of China, Hefei
[33]Sun Yat-Sen (Zhongshan) University, Guangzhou
[34]Joseph Henry Laboratories, Princeton University, Princeton, New Jersey, USA
[35]California Institute of Technology, Pasadena, California, USA
[36]Xi'an Jiaotong University, Xi'an
[37]Department of Physics, College of Science and Technology, Temple University, Philadelphia, Pennsylvania, USA
[38]Instituto de Física, Pontificia Universidad Católica de Chile, Santiago, Chile
[39]Nanjing University, Nanjing
[40]Department of Physics, Applied Physics, and Astronomy, Rensselaer Polytechnic Institute, Troy, New York, USA
[41]China Guangdong Nuclear Power Group, Shenzhen
[42]College of Electronic Science and Engineering, National University of Defense Technology, Changsha
[43]Iowa State University, Ames, Iowa, USA

(Dated: September 12, 2014)

A new measurement of the θ_{13} mixing angle has been obtained at the Daya Bay Reactor Neutrino Experiment via the detection of inverse beta decays tagged by neutron capture on hydrogen. The antineutrino events for hydrogen capture are distinct from those for gadolinium capture with largely different systematic uncertainties, allowing a determination independent of the gadolinium-capture result and an improvement on the precision of θ_{13} measurement. With a 217-day antineutrino data set obtained with six antineutrino detectors and from six 2.9 GW_{th} reactors, the rate deficit observed at the far hall is interpreted as $\sin^2 2\theta_{13} = 0.083 \pm 0.018$ in the three-flavor oscillation model. When combined with the gadolinium-capture result from Daya Bay, we obtain $\sin^2 2\theta_{13} = 0.089 \pm 0.008$ as the final result for the six-antineutrino-detector configuration of the Daya Bay experiment.

PACS numbers: 14.60.Pq, 29.40.Mc, 28.50.Hw, 13.15.+g
Keywords: neutrino oscillation, reactor, Daya Bay, hydrogen neutron capture

Neutrino oscillations are described by the three angles (θ_{13}, θ_{23}, θ_{12}) and phase (δ) of the PMNS matrix [1, 2]. Recent results [3–7] have established that θ_{13} is non-zero, as had been indicated by accelerator- and reactor-neutrino experiments [8–14]. Accurate and precise knowledge of θ_{13} is essential to forthcoming experiments to determine the neutrino mass hierarchy and to search for CP violation in the lepton sector [15]. Definite θ_{13} results were obtained by measuring the changes of reactor antineutrino rates and spectra at multiple sites via the inverse-beta decay (IBD) reaction, $\bar{\nu}_e + p \rightarrow e^+ + n$, in which the prompt e^+ signal is tagged by the delayed $\sim$8 MeV γ-cascade signal from neutron capture on gadolinium (nGd) [3–6]. In this Letter, with comparable statistics as the nGd case, a new measurement obtained by tagging the delayed 2.2 MeV γ from neutron capture on hydrogen (nH) [14, 16, 17] at Daya Bay is presented. New analysis approaches have been developed to meet the challenges associated with the higher background, longer neutron capture time ($\sim$200 μs), and a lower energy γ ray from neutron capture for nH IBD events. This nH analysis provides an independent measurement of $\sin^2 2\theta_{13}$, and leads to an improved precision on the θ_{13} mixing angle when combined with the nGd result obtained from the same period of the six antineutrino detector (AD) configuration [6]. The inclusion of nH capture results will improve the ultimate precision of Daya Bay for both θ_{13} and the $\bar{\nu}_e$ mass-squared difference $|\Delta m^2_{ee}|$ [6]. Optimization of the nH analysis method will be applicable to future reactor neutrino experiments that address the reactor-antineutrino anomaly [18–21] and determine the neutrino mass hierarchy [22–25].

A detailed description of the Daya Bay experiment can be found in [26, 27]. The ongoing experiment consists of two near experimental halls, EH1 and EH2, and one far hall, EH3. The power-weighted baselines to the six commercial power reactors are $\sim$500 m and $\sim$1.6 km for the near and far halls, respectively. In this analysis, EH1, EH2 and EH3 have two, one and three ADs, respectively. All ADs are submerged in water pools consisting of optically separated inner (IWS) and outer water shields (OWS), which also function as Cherenkov detectors to tag cosmic-ray muons. All ADs utilize an identical three-zone design with 20 tons of Gd-loaded liquid scintillator (GdLS) in the innermost zone, 22 tons of liquid scintillator (LS) in the middle zone to detect γ's escaped from GdLS, and 40 tons of mineral oil in the outermost zone where photo-multiplier tubes (PMTs) are installed. Unlike the nGd events, nH capture can occur both in the LS and the GdLS regions, resulting in more nH than nGd events before event selection. The trigger threshold for each AD was set at $\sim$0.4 MeV based on the logical OR of the number of over-threshold PMTs and the analog sum of their signals [28]. The vertex and energy were reconstructed utilizing the charge topological information collected by the PMTs. For a 2.2-MeV γ, the vertex res-

olutions were ∼8 cm in the x-y plane and ∼13 cm in the z direction in a Cartesian coordinate system with the origin at the AD center and the $+z$ axis pointing upwards. Detector simulation was based on GEANT4 [29] with the relevant physical processes validated [26]. All data from Dec. 24, 2011 to Jul. 28, 2012 were used for this analysis. The live time of each AD is listed in Table I.

All triggered events at each site were sequenced according to their time stamps after removing an instrumental background resulting from spontaneous light emission of PMTs [3, 5]. Because of the latency between detectors, events with time separations less than 2 μs in the same hall were grouped together for identifying cosmic-ray muons. A water-pool muon was defined as an event with the number of over-threshold PMTs >12 in the IWS or >15 in the OWS, while an AD (shower) muon had a visible energy greater than 20 MeV (2.5 GeV) in an AD. Table I lists the total muon rate per AD, R_μ, which was stable over the entire data-taking period. Due to the long lifetimes of muon spallation products, the AD events were required to occur at least 400 μs, 800 μs or 1 s after a water-pool, AD or shower muon, respectively. The visible energy for each AD event was also required to be greater than 1.5 MeV to reject the low-energy background. The surviving AD events were denoted as "good" events for further study. Coincident events were identified within a 399 μs time window, T_c, beginning at 1 μs after each prompt signal candidate [30]. This procedure classified all good events into single-coincidence, double-coincidence (DC), and multi-coincidence categories. Events in the latter category account for ∼2% of the total and were not included for further analysis.

Since the DC events were dominantly accidentally coincident background, especially in the far hall, a maximum distance of 50 cm between the prompt and delayed vertices was required, rejecting 98% of this background at the cost of a 25% acceptance loss. This cut was one of the major differences between the nH and the nGd analyses. Figure 1 (a) shows the prompt energy *vs.* the delayed energy for all the DC events after this cut in the far hall. The IBD bands are clearly seen for both the 2.2-MeV-nH and the 8-MeV-nGd cases. The measured nH peak was around 2.33 MeV with a resolution of 0.14 MeV. The offset from the true peak value arose from the nonlinear and nonuniform energy response, which was pegged to the nGd capture peak in the reconstruction. The γ's from ^{40}K and ^{208}Tl decays are observed around 1.5 and 2.6 MeV, respectively, and the continuous bands from 1.5 to 3 MeV are from the decay products of ^{238}U and ^{232}Th. The nH IBD candidates were obtained by requiring the prompt energy to be less than 12 MeV and the delayed energy to be within $\pm 3\sigma$ of the measured nH peak in each AD. The numbers of the candidates are listed in Table I.

The four identified backgrounds in the selected sample are accidental coincidences, cosmogenically produced fast neutrons and ^{9}Li/^{8}He, and neutrons from the retracted ^{241}Am-^{13}C calibration source. The delayed signals of the latter three are all from correlated neutron captures.

The following procedure was adopted for removing the accidental coincidence background. An accidental background sample (ABS) consisting of $N_{\rm ABS-tot}$ events was first generated by pairing two single events separated by at least 10 hours. The same distance and energy cuts were then applied to the ABS events, resulting in $N_{\rm ABS-cut}$ events. As shown in Fig. 1 (b), the ABS describes well the pattern of the low-energy region in Fig. 1 (a). The spectra of correlated events dominated by IBD, $N_{\rm IBD}(\xi)$, were then obtained by subtracting the accidental background from the DC events, $N_{\rm DC}$:

$$N_{\rm IBD}(\xi) = N_{\rm DC}(\xi) - R \cdot T_{\rm live} \cdot \frac{N_{\rm ABS-cut}(\xi)}{N_{\rm ABS-tot}}, \quad (1)$$

where ξ represents the quantity under study, such as the delayed energy, $T_{\rm live}$ is the live time of data-taking listed in Table I, and R is the random coincidence rate that can be written as [30]

$$R = R_s \times e^{-R_s T_c} \times R_s T_c e^{-R_s T_c}, \quad (2)$$

where R_s is the singles rate, $e^{-R_s T_c}$ gives the probability of no prior coincidence within T_c, and $R_s T_c e^{-R_s T_c}$ is the probability of a trigger from an accidental coincidence within T_c. Table I lists the average rate of the accidental background in eq. (2) for each AD.

While the statistical uncertainty of R_s is negligible, a systematic uncertainty is caused by the presence in the single event sample of a very small fraction of genuine correlated events for which either the prompt or the delayed event is not detected. The singles rate R_s was determined to be ∼22 Hz from the average of the good triggered event rates before and after excluding both the DC events and the multi-coincidence events. The systematic uncertainty in R_s, estimated from the difference of these two rates, was found to be 0.18%, 0.16% and 0.05% for the EH1, EH2 and EH3, respectively. The singles rate R_s was observed to have a slow downward trend (< 0.36%/day) immediately after an AD was installed in water and become stable after about four months. The slow variation of R_s was taken into account by performing the accidental subtraction, eq. (1), on a run-by-run basis, with each run lasting about two days.

Figure 1 (c) shows the delayed energy spectra for the DC events in the near and far halls after subtracting the accidental background. Very similar spectra, clearly showing the nH and nGd peaks, were observed for all ADs. The procedure of accidental background subtraction was validated by checking the distribution of distance between the prompt and delayed vertices as shown in Fig. 2. Simulation studies indicated IBD events rarely occurred with the prompt and delay vertices separated beyond 200 cm. Figure 2 shows a flat distribution consistent with zero for the region beyond 200 cm. The distribution of the difference of the delayed and prompt

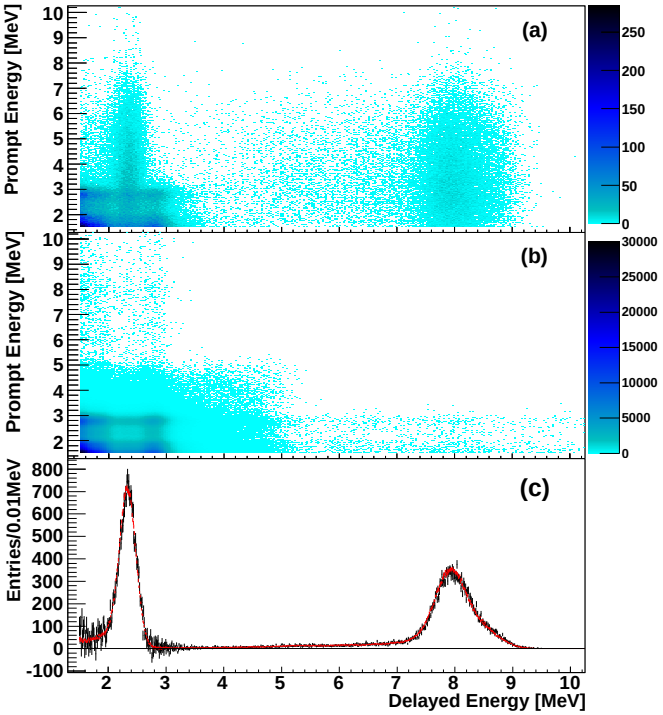

FIG. 1: (color online) (a) The prompt *vs.* delayed energy of double coincidence events with a maximum 50 cm vertex separation for all far-hall ADs, (b) the accidental background sample (ABS) events and (c) the delayed energy distribution after subtracting the accidentally coincident background for the far hall (black) and the near halls (red), where the total near site spectrum was normalized to the area of the far site spectrum.

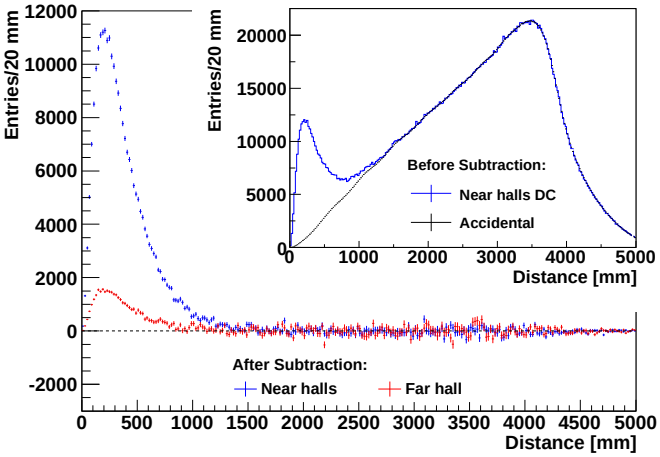

FIG. 2: (color online) Distributions of the distance between the prompt and the delayed vertices after the accidental background was subtracted for the near halls (blue) and the far hall (red). The inset plot shows the distance distributions for both the near halls double coincidence, DC, events (blue) and the expected accidental background sample (black).

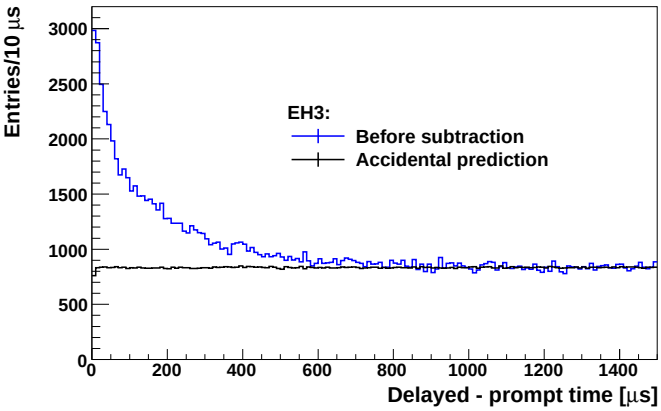

FIG. 3: (color online) Distribution of the delayed minus prompt time of the EH3 data sample. The blue histogram shows coincidences after all cuts except on the time difference. The black curve shows the predicted distribution for accidental coincidences.

times after all other cuts is shown in Fig. 3 to further validate the accidental subtraction and justify the 399 μs T_c cut. The accidental-background-subtracted spectra are consistent with no events of coincidence time longer than 1.5 ms.

The procedures for evaluating the ^{9}Li/^{8}He, fast neutron, and ^{241}Am-^{13}C backgrounds follow those in [3], except for three different selection cuts: the delayed energy cut, the distance cut, and an additional cut, $E > 3.5$ MeV, on the prompt energy to suppress the accidental background. The fast-neutron background is significantly higher than in the nGd case because the LS region is more accessible to the externally produced fast neutrons. The other two backgrounds are also slightly different due to detector geometry configuration. All background rates are listed in Table I.

The number of predicted IBD events, N, summed over various detector volumes v (GdLS, LS, and acrylic vessels) is given as

$$N = \phi\sigma\varepsilon_\mu\varepsilon_m \left[\sum_{v}^{\text{GdLS, LS, Acry.}} N_{p,v} f_v \varepsilon_{ep,v}\varepsilon_{ed,v}\varepsilon_{t,v}\right] \varepsilon_d, \quad (3)$$

where ϕ is the antineutrino flux, which was modeled as in [6], and N_p, σ and f are the number of protons, IBD cross section and hydrogen capture fraction, respectively. The efficiency ε_μ is the efficiency of the muon veto and ε_m is the efficiency of the multiplicity cut for the DC selection [30]. The efficiency ε_{ep} (ε_{ed}) is the prompt (delayed) energy cut efficiency, and ε_t (ε_d) refers to the efficiency of the time (distance) cut.

The θ_{13} analysis is based on relative rates, as in [3, 5], such that uncertainties that are correlated among ADs largely cancel and the uncorrelated uncertainties give the dominant contributions.

The central values of ε_{ep} and ε_{ed} were evaluated from the simulation. The prompt energy cut at 1.5 MeV

	EH1		EH2		EH3	
	AD1	AD2	AD3	AD4	AD5	AD6
Live time (day)	191.0	191.0	189.6	189.8	189.8	189.8
R_μ (Hz)	201.0	201.0	150.6	15.73	15.73	15.73
$\varepsilon_\mu\varepsilon_m$	0.7816	0.7783	0.8206	0.9651	0.9646	0.9642
Candidates	74136	74783	69083	20218	20366	21527
Accidental rate (/AD/day)	64.96 ± 0.13	64.06 ± 0.13	57.62 ± 0.11	62.10 ± 0.06	64.05 ± 0.06	68.20 ± 0.07
Fast n rate (/AD/day)	2.09 ± 0.56		1.37 ± 0.40		0.10 ± 0.04	
^{9}Li/^{8}He rate (/AD/day)	2.75 ± 1.38		2.14 ± 1.07		0.26 ± 0.13	
^{241}Am-^{13}C rate (/AD/day)	0.09 ± 0.05	0.09 ± 0.05	0.09 ± 0.05	0.06 ± 0.03	0.06 ± 0.03	0.06 ± 0.03
IBD rate (/AD/day)	426.71 ± 2.36	434.09 ± 2.37	382.69 ± 2.04	47.87 ± 0.79	46.78 ± 0.79	49.02 ± 0.82
nH/nGd	0.653 ± 0.004	0.654 ± 0.004	0.658 ± 0.004	0.653 ± 0.012	0.641 ± 0.012	0.679 ± 0.013

TABLE I: Summary of the hydrogen capture data sample. All the rate quantities are corrected with $\varepsilon_\mu\varepsilon_m$. The bottom row contains the ratio of the measured nH IBD rate to that of nGd from [6].

caused about 5% inefficiency in ε_{ep} for GdLS and LS events and a much higher loss in the acrylic. The slight variations in energy scale and resolution among different ADs introduced an uncorrelated uncertainty of 0.1%. For ε_{ed}, the 3-σ energy cut around the nH capture peak made the efficiency largely insensitive to the small variations of energy calibration and resolution. The efficiency ε_{ed} also included a small contribution from the low energy tail of nGd capture events. The uncertainty in ε_{ed} was determined by using a spallation neutron sample. Since the spallation neutron fluxes for neighboring ADs were nearly identical and the relative nGd acceptance in the GdLS region was accurately measured [3, 5], a comparison of the spallation neutron rates between nH and nGd captures gave an uncertainty of 0.5%. Simulations of IBD events in different ADs with as-built dimensions were also consistent with this uncertainty estimate.

The central value of ε_t was also evaluated with the simulation. The sources of the uncorrelated uncertainty include the number densities of various isotopes in LS and GdLS, the neutron elastic and capture cross sections, and the precision of time measurements. A chemical analysis showed that the density difference among the ADs is less than 0.1% and that the weight fractions of carbon and hydrogen among the ADs differed by less than 0.3%, limited by the instrumental precision. The uncertainty in number densities introduced a 0.1% uncorrelated uncertainty in ε_t. The precision of the timing measurement was studied using β-α coincident events from the decay chain of ^{214}Bi-^{214}Po-^{210}Pb originating from the ^{238}U cascade decays. With the same procedure of accidental subtraction applied, a comparison of the measured lifetime of ^{214}Po with the known value (237 μs) verified that the uncertainty on the timing precision due to the electronics was at the level of 0.1%. In total, the uncorrelated uncertainty was taken as 0.14%. A study of a clean nH IBD sample with the prompt energy >3.5 MeV for the ADs in the two near halls also confirmed this conclusion.

The central value of ε_d was directly measured from the distribution of the distance between the prompt and delayed vertices (see Fig. 2). The uncorrelated uncertainty, caused by the slight variations in the vertex reconstruction bias and resolution, was estimated to be 0.4%.

The value and uncertainty of N_p in GdLS were discussed in [26]. The proton number N_p in the LS region was determined in the same way and its uncorrelated uncertainty of 0.13% was dominated by the uncertainty of the Coriolis-mass-flow meter. The H-capture fraction, f, was less than unity due to neutron capture on Gd and C, and was estimated by the simulation to be 96% in the LS region and 16% in the GdLS region. The relative difference among ADs is negligible [5].

The selected nH IBD sample was about 65% of the size of the nGd IBD sample [6]. The total uncorrelated uncertainty per AD was 0.67% as summarized in Table II. The nH/nGd ratios among ADs 1, 2, and 3 agreed within 0.6% as shown in Table I, which provided a strong confirmation of the uncorrelated uncertainty per AD.

	Uncorrelated uncertainty	Coupled
$N_{p,\mathrm{GdLS}}$	0.03%	yes
$N_{p,\mathrm{LS}}$	0.13%	no
$N_{p,\mathrm{Acrylic}}$	0.50%	no
$\varepsilon_{ep,v}$	0.1%	yes
$\varepsilon_{ed,v}$	0.5%	no
$\varepsilon_{t,v}$	0.14%	yes
ε_d	0.4%	no
Combined	0.67%	

TABLE II: The per-AD relative uncorrelated uncertainty summary. The quoted uncertainties on the efficiencies are independent of volume. The combined uncertainty takes into account the relative GdLS, LS and acrylic masses. The last column indicates whether the uncorrelated uncertainties for the nH and nGd analyses are coupled.

Figure 4 shows a comparison of the prompt spectra of the far hall and the near halls weighted by the near-to-far baseline ratio, along with the ratio of the measured-to-predicted rates as a function of baseline. Clear evidence for electron antineutrino disappearance is observed. A χ^2 with pull terms for nuisance parameters as in [3, 5] is minimized to extract $\sin^2 2\theta_{13}$ from the detected nH IBD rate deficit. The value of $|\Delta m^2_{31}|$ is taken from MINOS [31]. The best fit is $\sin^2 2\theta_{13}$=0.083 ± 0.018 with

χ^2=4.5 for 4 degrees of freedom. The increase in χ^2 is 20 when θ_{13} is set to zero, ruling out this null assumption at 4.6 standard deviations. The expected Far/Near ratio based on the best-fit $\sin^2 2\theta_{13}$ value is compared to data in Fig. 4.

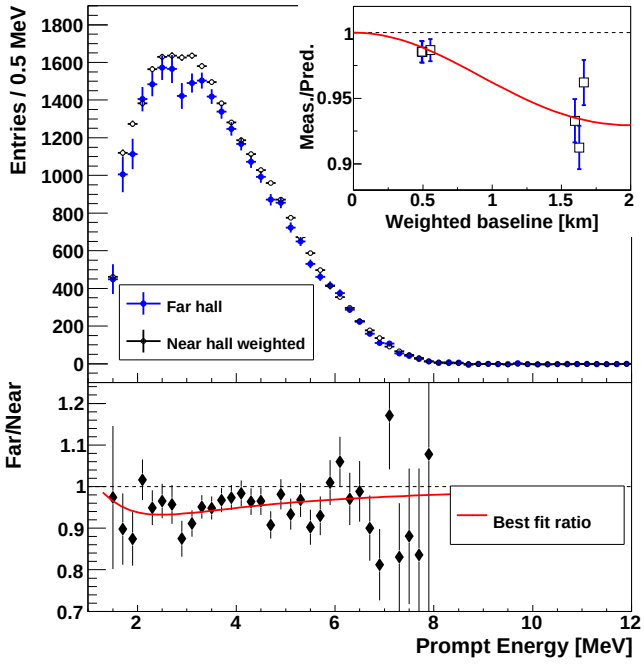

FIG. 4: (color online) The detected energy spectrum of the prompt events of the far hall ADs (blue) and near hall ADs (open circle) weighted according to baseline. The far-to-near ratio (solid dot) with best fit θ_{13} value is shown in the lower plot. In the inset is the ratio of the measured to the predicted rates in each AD *vs.* baseline, in which the AD4 (AD6) baseline was shifted relative to that of AD 5 by 30 (−30) m.

The nH result is an independent measurement of θ_{13} and provides a strong confirmation of the earlier measurement using nGd [6]. Currently both the nH and nGd [6] uncertainties are statistics-dominated. With only statistical uncertainties considered in the nH fit, the uncertainty of $\sin^2 2\theta_{13}$ is 0.015, about 70% of the total uncertainty when uncertainties are added in quadrature, which is the same for the nGd analysis. The dominant systematic uncertainties are also independent of the nGd analysis. For example, the delayed-energy cut is uncoupled (uncorrelated) because the impact of the relative energy-scale difference on the fixed-energy threshold in the nGd analysis [3, 5, 6] is avoided with the data-driven 3-σ cut. Further couplings are noted in the Table II. With all uncoupled uncertainties included in the nH fit, the uncertainty of $\sin^2 2\theta_{13}$ is 0.017 (90% of the total uncertainty in quadrature). By conservatively taking all coupled quantities to be fully coupled, the correlation coefficient is about 0.05, indicating an essentially independent measurement of θ_{13}. The weighted average of nH and nGd [6] results is 0.089 ± 0.008, improving the nGd result precision by about 8%.

In summary, with an nH sample obtained in the six-AD configuration, by comparing the rates of the reactor antineutrinos at the far and near halls at Daya Bay, we report an independent measurement of $\sin^2 2\theta_{13}$ which is in good agreement with the one extracted from the minimally correlated nGd sample. By combining the results of the nH and nGd samples, the precision of $\sin^2 2\theta_{13}$ is improved. In general, with different systematic issues, results derived from nH samples will be important when the nGd systematic uncertainty becomes dominant in the future. It is also expected that nH analysis will enable other neutrino measurements [18, 22].

Daya Bay is supported in part by the Ministry of Science and Technology of China, the United States Department of Energy, the Chinese Academy of Sciences, the National Natural Science Foundation of China, the Guangdong provincial government, the Shenzhen municipal government, the China General Nuclear Power Corporation, Key Laboratory of Particle & Radiation Imaging (Tsinghua University), Ministry of Education, Key Laboratory of Particle Physics and Particle Irradiation (Shandong University), Ministry of Education, Shanghai Laboratory for Particle Physics and Cosmology, the Research Grants Council of the Hong Kong Special Administrative Region of China, University Development Fund of The University of Hong Kong, the MOE program for Research of Excellence at National Taiwan University, National Chiao-Tung University, and NSC fund support from Taiwan, the U.S. National Science Foundation, the Alfred P. Sloan Foundation, the Ministry of Education, Youth and Sports of the Czech Republic, the Joint Institute of Nuclear Research in Dubna, Russia, the CNFC-RFBR joint research program, National Commission of Scientific and Technological Research of Chile, and Tsinghua University Initiative Scientific Research Program. We acknowledge Yellow River Engineering Consulting Co., Ltd. and China railway 15th Bureau Group Co., Ltd. for building the underground laboratory. We are grateful for the ongoing cooperation from the China General Nuclear Power Corporation and China Light & Power Company.

[1] B. Pontecorvo, Sov. Phys. JETP **6**, 429 (1957) and **26**, 984 (1968).
[2] Z. Maki, M. Nakagawa, and S. Sakata, Prog. Theor. Phys. **28**, 870 (1962).
[3] F. P. An *et al.* (Daya Bay collaboration), Phys. Rev. Lett. **108**, 171803 (2012).
[4] J. K. Ahn *et al.* (RENO collaboration), Phys. Rev. Lett. **108**, 191802 (2012).
[5] F. P. An *et al.* (Daya Bay collaboration), Chinese Phys. C **37**, 011001 (2013).
[6] F. P. An *et al.* (Daya Bay collaboration), Phys. Rev. Lett. **112**, 061801 (2014).
[7] K. Abe *et al.* (T2K Collaboration) Phys. Rev. Lett. **112**, 061802 (2014).
[8] K. Abe *et al.* (T2K collaboration), Phys. Rev. Lett. **107**, 041801 (2011).
[9] P. Adamson *et al.* (MINOS collaboration), Phys. Rev. Lett. **107**, 181802 (2011).
[10] P. Adamson *et al.* (MINOS collaboration), Phys. Rev. Lett. **110**, 171801 (2013).
[11] A. Gando *et al.* (KamLAND collaboration), Phys. Rev. D **83**, 052002 (2011).
[12] Y. Abe *et al.* (Double Chooz collaboration), Phys. Rev. Lett. **108**, 131801 (2012).
[13] Y. Abe *et al.* (Double Chooz collaboration), Phys. Rev. D **86**, 052008 (2012).
[14] Y. Abe *et al.* (Double Chooz collaboration), Phys. Lett. B **723**, 66 (2013).
[15] C. Adams *et al.* (LBNE collaboration), arXiv:1307.7335 (2013).
[16] K. Eguchi et al. (KamLAND Collaboration), Phys. Rev. Lett. **90**, 021802 (2003).
[17] H. Zhang *et al.* (Super-Kamiokande collaboration), Astropart. Phys. **60**, 41 (2015).
[18] T. A. Mueller *et al.*, Phys. Rev. C **83**, 054615 (2011).
[19] P. Huber, Phys. Rev. C **84**, 024617 (2011).
[20] M. Fallot *et al.*, Phys. Rev. Lett. **109**, 202504 (2012).
[21] A.C. Hayes, J.L. Friar, G.T. Garvey, and Guy Jonkmans, arXiv:1309.4146 (2013).
[22] S.T. Petcov and M. Piai, Phys. Lett. B **533**, 94 (2002).
[23] S. Choubey, S.T. Petcov and M. Piai, Phys. Rev. D **68**, 113006 (2003).
[24] J. G. Learned, S. T. Dye, S. Pakvasa and R. C. Svoboda, Phys. Rev. D **78**, 071302(R) (2008).
[25] L. Zhan, Y. Wang, J. Cao, and L. Wen, Phys. Rev. D **78**, 111103(R) (2008).
[26] F. P. An *et al.* (Daya Bay collaboration), Nucl. Instr. Meth. A **685**, 78 (2012).
[27] F. P. An *et al.* (Daya Bay Collaboration), arXiv:hep-ex 0701029.
[28] H. Gong *et al.*, Nucl. Instr. Meth. A **637**, 138 (2011).
[29] S. Agostinelli *et al.*, Nucl. Instr. Meth. A **506**, 250 (2003) and Allison, J. *et al.*, IEEE Trans. Nucl. Sci. **53**, 270 (2006).
[30] J. Yu, Z. Wang, and S. Chen, arXiv:1301.5085 (2013).
[31] P. Adamson *et al.* (MINOS Collaboration), Phys. Rev. Lett. **106**, 181801 (2011).